



The Air-Gap PAD: A Roll-to-Roll-Compatible Fabrication Method for Paper Microfluidics

Journal:	<i>Lab on a Chip</i>
Manuscript ID	LC-ART-12-2022-001164.R1
Article Type:	Paper
Date Submitted by the Author:	21-Feb-2023
Complete List of Authors:	Roller, Rachel; University of Notre Dame, Chemistry and Biochemistry Rea, Angela; University of Notre Dame, Chemistry and Biochemistry Lieberman, Marya; University of Notre Dame, Department of Chemistry and Biochemistry

ARTICLE

The Air-Gap PAD: A Roll-to-Roll-Compatible Fabrication Method for Paper Microfluidics

Rachel M. Roller,^a Angela Rea^a and Marya Lieberman^{a*}

Received 20th December 2022,
Accepted 00th January 20xx

DOI: 10.1039/x0xx00000x

Paper-based analytical devices (PADs) offer a low-cost, user-friendly platform for rapid point-of-use testing. Without scalable fabrication methods, however, few PADs make it out of the academic laboratory and into the hands of end users. Previously, wax printing was considered an ideal PAD fabrication method, but given that wax printers are no longer commercially available, alternatives are needed. Here, we present one such alternative: the air-gap PAD. Air-gap PADs consist of hydrophilic paper test zones, separated by “air gaps” and affixed to a hydrophobic backing with double-sided adhesive. The primary appeal of this design is its compatibility with roll-to-roll equipment for large-scale manufacturing. In this study, we examine design considerations for air-gap PADs, compare the performance of wax-printed and air-gap PADs, and report on a pilot-scale roll-to-roll production run of air-gap PADs in partnership with a commercial test-strip manufacturer. Air-gap devices performed comparably to their wax-printed counterparts in Washburn flow experiments, a paper-based titration, and a 12-lane pharmaceutical screening device. Using roll-to-roll manufacturing, we produced 2,700 feet of air-gap PADs for as little as \$0.03 per PAD.

Introduction

Microfluidic paper analytical devices, or μ PADs, are a promising platform for point-of-use testing because of their low cost, portability, rapid results, and ease of use. A landmark article by the Whitesides group in 2007¹ sparked an explosion of research interest in μ PADs for applications as far-reaching as environmental monitoring,^{2–5} chemical education,^{6–14} pharmaceutical screening,^{15–22} and point-of-care diagnostics.^{23–25} Despite the large number of published academic articles on μ PADs, however, very few μ PADs have made it out of the academic laboratory and into the real world.^{26,27} One key reason for the difficulty of this “benchtop-to bedside” transition is the lack of scalable fabrication methods for paper microfluidics.²⁷

Fabrication methods have been an ongoing challenge for the field of paper microfluidics since its inception. Early μ PADs relied on photolithography,¹ which requires expensive materials, specialized equipment, and trained personnel. Many of the laboratory-based methods developed since, such as silanization,²⁸ chemical vapor deposition,²⁹ and plasma treatment,^{30,31} suffer from the same issues. Others, like hand cutting,^{32,33} hand drawing,^{34–36} hand folding,³⁷ plotting,^{38–40} craft cutting,⁴¹ 3D printing,^{42,43} stamping,^{44–49} wax dipping,⁵⁰ spraying,^{51,52} and screen printing,^{53–56} boast low cost and require little equipment, but still suffer from low throughput

and high hands-on labor. When wax printing was applied to μ PAD fabrication, it was soon heralded as the method of choice for μ PAD fabrication due to its reasonable cost, moderate throughput, simple operation, and ease of prototyping.^{34,57} In 2016, however, Xerox discontinued its line of solid-ink printers, and no other company has picked up the technology. Other printer-based methods, like laser printing,^{58–61} inkjet printing,^{62–68} and recently, thermal transfer printing,⁶⁹ have been explored as potential alternatives to wax printing, but remain most suitable for mid-scale applications requiring only moderate throughput.

Roll-to-roll manufacturing⁷⁰ offers continuous, in-line processing for large-scale production of microfluidic devices.^{71,72} Roll-to-roll manufacturing has been used to produce lateral flow assays, aquarium test strips, urine test strips, and pH strips for years, but few researchers have applied this technology to μ PAD fabrication. One roll-to-roll method, flexographic printing, was explored by Olkkonen et al.⁷³ and Määttä et al.⁶⁴ to pattern paper with hydrophobic barriers made of polystyrene⁷³ or PDMS-based⁶⁴ ink. A smaller-scale roll-to-roll liquid flame spray technique was reported by Songok et al.,⁷⁴ and roll-to-roll thermal transfer printing was used by Liu et al. to pattern paper with wax.⁷⁵

The air-gap PAD sprang from the need to find a scalable alternative to wax printing. Air-gap PADs consist of paper test zones affixed to a hydrophobic backing; the spaces between test zones provide an “air gap” that the liquid cannot cross. Similar devices made of paper affixed to a hydrophobic backing have been characterized previously,^{76–78} but the possibility of mass-producing air-gap devices had yet to be explored.

As a proof of concept, we chose to target our lab’s two most commonly made device designs: the 12-lane PAD and the

^a University of Notre Dame, Department of Chemistry and Biochemistry, Notre Dame, IN, 46556.

* To whom correspondence should be addressed: mlieberm@nd.edu
Electronic Supplementary Information (ESI) available: Supplemental figures and tables, raw data. See DOI: 10.1039/x0xx00000x

paper titrator. The 12-lane PAD was developed to screen for substandard and falsified pharmaceuticals in low- and middle-income countries,^{11,15–19} and has since been adapted to screen chemotherapy agents^{21,22,79,80} and illicit drugs.⁸¹ The paper titrator was developed to enable hands-on, inquiry-based analytical chemistry labs for distance learning.¹² Each 12-lane PAD is individually serialized (starting at 10,000), and as of the time of this writing, the serial numbers had just crossed the 70,000 mark, which means that ~7,500 12-lane PADs have been produced each year since 2014; we have also produced over 34,000 titrators since 2020. For both of these devices, then, scalability was a top priority. Thus, while the air-gap PAD can be made by hand for prototyping purposes, it is designed to be compatible with large-scale roll-to-roll manufacturing.

In this study, we investigate design considerations (dimensions, wetting behavior, reagent compatibility) of the air-gap PAD and compare the performance of wax-printed and air-gap versions of 12-lane PADs and paper titrators. We also report on a pilot-scale roll-to-roll production run of air-gap PADs.

Experimental

PAD fabrication

Air-gap PADs can be assembled by hand for prototyping, or mass produced using a roll-to-roll method.

Hand fabrication. To fabricate the air-gap devices by hand for prototyping purposes, Ahlstrom 319 fast chromatography paper (Midland Scientific, Chicago, IL) was backed with double-sided pressure-sensitive adhesive (Artgrafix, Beacon Falls, CT) and cut into strips with a Glowforge Basic laser cutter. These strips were mounted on a plastic backing using a pegboard for alignment (see Figure S1). The assembly was then sliced crossways into air-gap devices (see Figure 1).

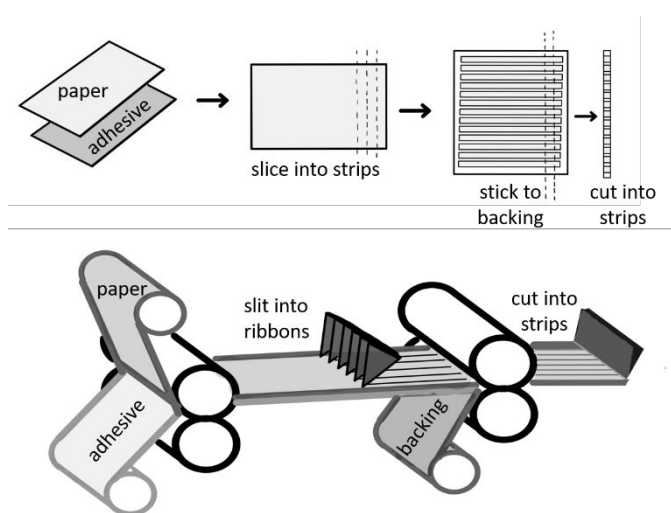


Figure 1. Air-gap PAD fabrication. Top: Chromatography paper is backed with double-sided adhesive, cut into strips, applied to hydrophobic backing with air gaps between each paper strip, and sliced crossways into air-gap devices. Bottom: Simplified schematic of the roll-to-roll manufacturing process.

Roll-to-roll production. For the roll-to-roll manufacturing, we collaborated with Serim Research Corporation, a test-strip manufacturer in Elkhart, IN. For this method, a 500-ft roll of 8-inch-wide Ahlstrom 319 paper was dry-laminated with double-sided adhesive (3M double-coated tape 415, 3M, Saint Paul, MN) and slit into 0.2-inch ribbons. Seven of these ribbons were laminated onto a roll of 3.25-inch-wide white, hydrophobically coated polystyrene (Trycite, Franklin Park, IL, lot # 1345300) with 9-mm spacing and cut crossways into 9-inch cards. These 9-inch cards were further cut into either 3-inch cards or 0.2-inch strips. Before cutting, the back of the polystyrene was laminated with double-sided adhesive so that test strips could be attached to custom-printed card holders.

PAD characterization and design considerations

Three different backing types with varying degrees of hydrophobicity were assessed for their performance in the air-gap devices: commercial overhead transparency film (C-line, Mt Prospect, IL) and both the coated and uncoated sides of Trycite® polystyrene film (Transcendia, Franklin Park, IL). Measurement with a contact angle goniometer (DropMaster DMO-701, Kyowa Interface Science Co., Japan) using the sessile drop method on nine replicates, analyzed using the tangent method in FAMAS software showed that the transparency film was moderately hydrophilic ($\theta = 64^\circ \pm 2^\circ$), the uncoated side of the white film was on the border between hydrophobic and hydrophilic ($\theta = 87^\circ \pm 6^\circ$), and the coated side of the white film was strongly hydrophobic ($\theta = 140^\circ \pm 4^\circ$) (see Figure S2).

Three design variables were considered for their effect on device volume: paper area, air gap width, and backing hydrophobicity. Paper squares measuring 2.5 x 2.5 mm, 5 x 5 mm, and 7.5 x 7.5 mm were placed on the three backing types (transparency film, coated and uncoated polystyrene) with air gaps of 1, 2, and 3 mm. Deionized water was added to two adjacent paper squares in 10- μ L increments until the surface tension broke or the adjacent droplets merged.

Air-gap devices were also tested for their ability to contain other liquids, including simulated blood (Type A, Ward's Science, VWR, St. Catherine, Ontario), synthetic urine (RICCA Chemical Company, Arlington, TX), TWEEN® 20 (Sigma-Aldrich) surfactant solutions (2%, 5%, 10%, 20%, and 50%), ethanol, methanol, isopropanol, acetonitrile, acetone, and hexanes.

Washburn flow

To compare the wet-out behavior of the air-gap devices to that of wax-printed μ PADs, air-gap devices (2.5-, 5-, and 7.5-mm strips on moderately hydrophilic transparency film or on hydrophobic Trycite® polystyrene film) and wax-printed devices (2.5-, 5-, and 7.5-mm paper lanes separated with wax barriers, 1 mm before baking, 1.25 mm after baking) were placed on end in 1 cm deionized water tinted with blue food coloring (FD&C Blue 1, McCormick, Duluth, GA) and filmed for two minutes. To study the effect of lamination on the air-gap PADs, devices were laminated with clear packing tape (Scotch Heavy Duty Packing Tape, Office Depot) to within 1 cm of the bottom of the PAD. Video frames were analyzed at 1, 2, 5, and 10 seconds and at

10-second intervals thereafter to track the flow of liquid up the paper lanes. Wet-out behavior was then quantified using the Washburn Equation:

$$L = \sqrt{\frac{\gamma r \cos(\theta)}{2\eta} t}$$

which models the distance L traveled by a liquid with surface tension γ and viscosity η through a medium with pore radius r and contact angle θ in time t .^{82,83} Twelve replicate measurements were taken of each type of device.

Titrator testing

The air-gap device's performance as a vehicle for paper-based titrations was compared to the wax-printed titrator device described by Roller et al.¹² Both the wax-printed and air-gap titrators were pre-loaded with 5 μ L per square of *p*-toluenesulfonic acid (Alpha Aesar, Ward Hill, MA) solutions ranging from 100 mM to 3 M (see Figure 3 below). 40 μ L of 0.10 M sodium hydroxide (Fisher Scientific, Fair Lawn, NJ) with phenolphthalein indicator (HiMedia Laboratories, Dindori, India, 1-2 drops of 5% indicator solution per 10 mL analyte) was then added to each square to perform the limit titration. Four replicates of each device type were imaged and analyzed in ImageJ⁸⁴ to obtain titration curves. The green channel (G) was chosen for the titration curves as it is a close proxy for measuring the absorbance of the pink phenolphthalein solutions.

12-lane PAD testing

To compare the air-gap device's potential as an alternative to the wax-printed 12-lane PAD developed by the Lieberman lab for pharmaceutical analysis,¹⁵ air-gap PADs were fabricated (2.5-mm-wide laser-cut paper strips spaced 2 mm apart on transparency film) and stamped with the reagents specified by Bliese et al.¹⁷ Five active pharmaceutical ingredients (APIs) were tested: amoxicillin, ciprofloxacin, isoniazid, pyrazinamide, and rifampicin. Five PADs were run for each API. Images of the PADs were captured, rectified, and classified by a neural network⁸⁵ using a cell phone app.⁸⁶ For image capture by the app, transparency-film-based air-gap PADs were placed atop a piece of paper printed with the fiducial markings normally printed on the PAD itself.⁸⁵ The fiducials allow the app to recognize, align, and rectify the captured image. Each PAD was imaged against both dark and white background with four different devices—an iPhone, an iPad, a Google Pixel, and a Nokia phone—to obtain a total of 200 images. Blinded images of all 25 PADs (one image per PAD) were also read by eye by five trained users.

Results and discussion

Initial testing involved hand-fabricating air-gap devices to optimize device dimensions and materials. Prototype air-gap devices (12-lane PADs and titrators) were then compared to their wax-printed counterparts to ensure comparable assay performance. Finally, a pilot-scale production run was

conducted using roll-to-roll equipment in partnership with a commercial test-strip manufacturer.

PAD design and characterization

The maximum volume held by a single square of the air-gap device varied linearly with the area of the paper ($R^2 = 0.998$) with a constant air gap width (Figure S3). When the air gap width was increased from 1 mm to 2 mm, the maximum volume of all tested paper areas increased (see Figure S4), but a further increase from 2 mm to 3 mm did not significantly increase the capacity. This was due to the fact that with a small air gap, the paper test zones were so close to each other that adjacent droplets merged with each other as they grew too large, limiting the maximum volume. With a larger air gap, however, the droplets were farther apart, so the capacity depended only on the area of the paper test zones.

The hydrophobicity of the backing did not significantly affect the maximum volume of the device (see Figure S5). This is likely due to the water remaining "pinned" to the hydrophilic paper rather than on the backing. In functional use, however, the titration devices with more-hydrophobic backing material were less likely to leak when jostled, so the hydrophobically coated polystyrene film was used for titration experiments and the pilot-scale roll-to-roll production run.

The air-gap barriers successfully contained all tested aqueous solutions, including surfactant solutions, simulated blood, and synthetic urine, but could not contain organic liquids such as ethanol, methanol, isopropanol, acetonitrile, acetone, and hexane.

Washburn flow

As seen in Figure 2, the wet-out behavior of the unlaminated air-gap devices was comparable to that of the wax-printed PADs. When the distance traveled by the liquid was plotted against the square root of time according to the Washburn equation, the 5-mm wax-printed devices, transparency-film air-gap devices, plain and laminated hydrophobic Trycite[®] polystyrene air-gap devices, and 0.2-in plain and laminated roll-to-roll-fabricated devices gave linear graphs ($R^2 = 0.9976$, 0.9984, 0.9974, 0.9961, 0.9965, and 0.9916 respectively). The slopes of the wax-printed, transparency-film, and Trycite devices were identical within error according to Excel's LINEST function (0.504 ± 0.007 for wax-printed, 0.510 ± 0.006 for transparency-based air-gap, 0.500 ± 0.007 for hydrophobic Trycite[®] polystyrene-based air-gap, and 0.495 ± 0.008 for roll-to-roll air-gap).

Laminating the air-gap devices with packing tape, however, increased the rate of fluid flow, resulting in a steeper slope (0.655 ± 0.004 for laminated handmade device, 0.572 ± 0.015 for laminated roll-to-roll device). In 100 seconds, the water traveled 6.1 cm up the laminated lanes, but only 4.9 cm up the unlaminated lanes. This is consistent with previous literature reports of faster flow rates in laminated devices.^{78,87} The 7.5-mm lanes of the air-gap and wax-printed devices gave similar slopes to the 5-mm (unlaminated) devices (0.536 ± 0.008 for transparency-based air-gap, 0.498 ± 0.006 for hydrophobic Trycite[®] polystyrene-based air-gap, and 0.511 ± 0.01 for wax-

printed). This suggests that the inherent wetting properties of the paper are not noticeably affected by the differences between the air-gap and wax-printing fabrication methods or by the hydrophobicity of the backing, but if more rapid fluid flow is desired, the device can be laminated.

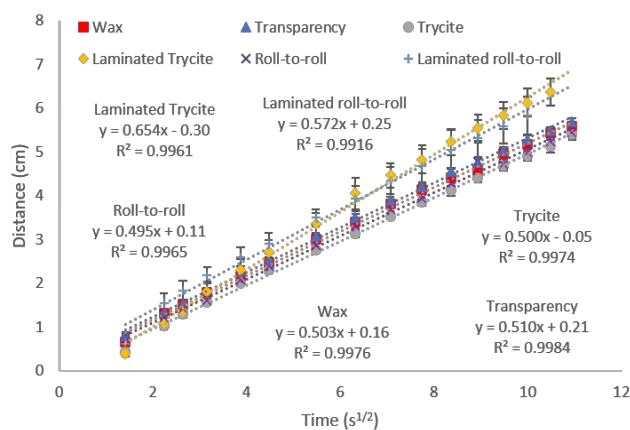


Figure 2. Washburn flow plots of air-gap (transparency film, hydrophobic Trycrite polystyrene, Trycrite laminated with packing tape, roll-to-roll, and roll-to-roll laminated with packing tape) and wax-printed devices with 5mm lanes. Error bars show standard deviation of 12 measurements.

Titration performance

When a wax-printed titrator, a prototype air-gap titrator, and a roll-to-roll air-gap titrator preloaded with *p*-toluenesulfonic acid were compared side-by-side in a titration with 40 μ L of 0.10 M sodium hydroxide analyte and phenolphthalein indicator, the air-gap and wax-printed devices performed virtually identically (see Figure 3).

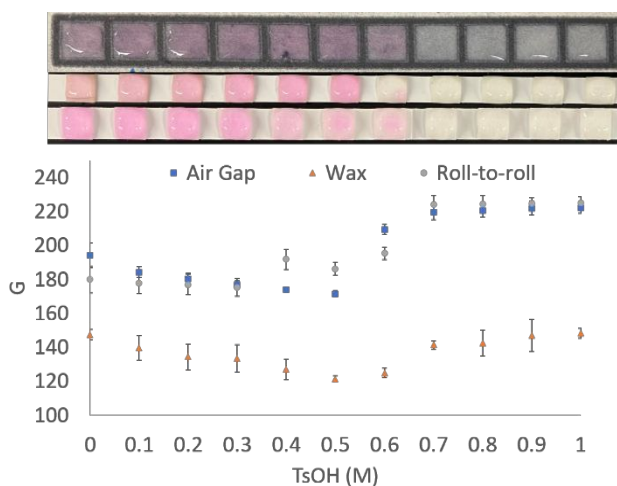


Figure 3. Comparison of wax-printed (top), prototype air-gap (2nd row), and roll-to-roll air-gap (3rd row) titrators. Each square of the devices was loaded with 5 μ L of the specified concentration of *p*-toluenesulfonic acid. 40 μ L of 0.1 M sodium hydroxide with phenolphthalein was added to each square and mixed with a pipette to re-dissolve the stored TsOH. All titrators gave an endpoint (first clear, non-pink bubble) at the 700 mM TsOH square (the theoretical equivalence point was the 800 mM TsOH square). Bottom: Titration curves obtained from ImageJ analysis of wax-printed and air-gap titrators. The endpoint occurs where the graph levels off, not at the inflection point. Error bars show standard deviations of 4 replicates.

Unlike a typical pH-vs-volume titration curve, where equivalence is found at the inflection point, the endpoint for these titration curves is found at the point where the graph levels off, signaling complete disappearance of the pink color of the phenolphthalein indicator. The exact RGB values obtained by ImageJ analysis were different, as the black wax backing of the wax-printed devices resulted in a darker background color than the white backing of the air-gap devices. Because the air-gap devices do not have interference from the color of the backing, they had less variability in the measured color intensity and therefore smaller error bars. The endpoints, however, were the same for all three device types, both by visual inspection and titration curve (Figure 3).

12-lane PAD performance

Images of the 12-lane pharmaceutical screening PADs were captured using a mobile app⁸⁶ and analyzed using a neural network to identify the active pharmaceutical ingredient as described in Banerjee et al.⁸⁵ The mobile app⁸⁶ successfully captured and rectified images of the air-gap PADs (192 images total). Example images of air-gap and wax-printed PADs are shown in Figure 4; see Figure S6 for images of all 25 PADs. Neither the app operating system (iOS vs Android, *p*-value = 0.66) nor the background color (black vs white, *p*-value = 0.51) significantly affected the accuracy of the neural network (see Table S1 for Student's *t*-tests).

The neural network struggled to accurately classify the APIs present in the images of the air-gap PADs (64% accuracy for air-gap vs 98% accuracy for wax-printed; see Table 1). This was not surprising, as the neural network was trained using only wax-printed PAD images. To confirm that the decrease in accuracy was due to the neural network and not to defects in the air-gap PADs themselves, 25 blinded air-gap PAD images (one image for each card) were analyzed by five trained human readers. When the PADs were classified by eye, four out of five readers classified all 25 cards correctly, and the overall average accuracy was 97% (see Table 1).

Table 1. Classification accuracy of wax-printed and air-gap pharmaceutical screening PADs.

API	Wax-printed accuracy (%) (app/neural net)	Air-gap accuracy (%) (app/neural network)	Air-gap accuracy (%) (human readers)
Amoxicillin	99	57	100
Ciprofloxacin	92	72	100
Isoniazid	100	80	100
Pyrazinamide	100	45	88
Rifampicin	100	68	96
Average \pm Standard Deviation	98 \pm 4	64 \pm 14	97 \pm 5

For both human readers and the cell-phone app, pyrazinamide was the most difficult drug of the five APIs studied to classify correctly, most likely because its "color barcode" consists of only one distinct color change (a dark red color in

lane G), which can be easy to overlook. Isoniazid, in contrast, gives distinct color changes in five lanes, which makes it easier to classify accurately. One potential reason for amoxicillin's low accuracy on the app but high accuracy with human readers is that one of its three color changes (the red "flame" in lane K) can be unreliable if the PAD has been stored for several months. A human reader can still reliably identify amoxicillin based on the other two predicted color changes, but a neural network may struggle. Another potential explanation for the differences in accuracy between the app and human readers is the fact that the paper strips in the prototype air-gap PADs had a small amount of browning from the laser-cutting process, which altered the shade of the colors slightly. (As the roll-to-roll process uses knives rather than a laser cutter, this is not an issue for scaled-up air-gap manufacturing.) For a neural network, this alteration in color intensity is problematic, but a human reader can still readily identify the colors.

Our results, then, show that the air-gap PAD performed comparably to the wax-printed PAD when analyzed by human readers. Since the PADs were originally developed to be read by eye and can be reliably used without the cell-phone app and neural network,^{15–18,22} this shows that the air-gap PADs are a viable successor to the wax-printed 12-lane PADs. Our challenges when attempting to analyze the air-gap PADs with a neural network designed for wax-printed PADs, however, highlight the fact that changing external factors, like the fabrication method, will likely necessitate retraining any neural networks used for computer-assisted classification. We anticipate that retraining our neural network on images of air-gap PADs will ameliorate many of these issues and improve the accuracy of the cell-phone app's classification.



Figure 4. Wax-printed and air-gap pharmaceutical screening PADs. Left panels show wax-printed 12-lane PADs for ciprofloxacin (top) and isoniazid (bottom) with expected color changes circled. Right panels show air-gap PADs for ciprofloxacin (top) and isoniazid (bottom). Images of all 25 air-gap PADs read by the human evaluators can be found in the supplemental information.

Roll-to-roll production run

We partnered with a local test-strip manufacturer to perform a pilot roll-to-roll production run of the air-gap devices. Because we use a 96-well inoculator or a multichannel pipette to deposit reagents, the paper lanes needed to be spaced at 9mm, and thus two paper guides were custom machined (\$3400, one-time

cost) with this spacing. Excluding the one-time cost of the guides, the total cost for materials, equipment use, and labor was ~\$4,500. A 500-ft roll of 8-in paper produced approximately 2,700 feet of assembled cards, which translates to either 10,800 3-in cards for pharmaceutical screening or 162,000 1/8-in test strips for paper-based titrations. This brings the cost per device to \$0.41 per 3-in PAD (\$0.73, including one-time costs) or \$0.026 per 1/8-in titrator (\$0.05, including one-time costs).

Our manufacturing partner's current equipment is limited to a maximum of seven paper lanes no narrower than 0.2 inches. The current 7-lane PADs are useful for the paper titrators¹² and a pared-down version of the PAD used for illicit drug analysis,⁸¹ but in future production runs, we plan to obtain a knife set capable of cutting 2.5mm lanes, as well as another custom guide that can deposit 12 paper strips at a time so we can mass produce the 12-lane pharmaceutical PADs.

Conclusions

The air-gap design offers a simple, scalable alternative to traditional methods of fabricating paper microfluidics. Air-gap devices can be readily fabricated by hand for prototyping and device development, but more importantly, we have shown that they can be mass produced with roll-to-roll manufacturing. Since the necessary roll-to-roll equipment is commonly available at many test-strip manufacturers, it is possible to partner with a company to produce air-gap devices at scale without purchasing manufacturing equipment. At the pilot-manufacturing scale, the cost of air-gap device fabrication was as low as \$0.03 per device, including labor, equipment use, and raw materials.

This roll-to-roll method can create PADs consisting of straight paper channels and square dot features. Further development will be needed to create more general designs with curved lines, holes, and complex shapes, or to incorporate folded, rolled, or stacked multi-level structures which are readily accessible by other fabrication methods. The current method, however, is applicable not only to our two device designs, the paper titrator¹² and the 12-lane PAD,^{11,15,17,19,21,81,85,88} but also to the many PADs reported by other groups that involve spot tests and/or straight channels.^{6,8,36,44,52,55,64–66,74,89–95}

Our testing showed that air-gap devices performed comparably with wax-printed devices for paper-based titrations and pharmaceutical screening. Future research will focus on training our neural network to recognize air-gap pharmaceutical screening devices and expanding the air-gap method to other device architectures.

Author Contributions

Rachel M. Roller: Conceptualization, Methodology, Validation, Investigation, Formal analysis, Writing - Original Draft, Review and Editing, Visualization. **Angela Rea:** Investigation, Validation. **Marya Lieberman:** Conceptualization, Writing - Review and Editing, Supervision, Project administration, Funding acquisition.

Conflicts of interest

Marya Lieberman is the founder and CEO of Paper Analytics, LLC, a not-for-profit organization that sells paper labware for educational and pharmaceutical screening purposes at cost. Provisional patent application 63/373,059 has been filed for the air-gap method of fabricating paper microfluidic devices.

Acknowledgements

This work was partially supported by a grant from the Howard Hughes Medical Institute under the MICRO Project and by the National Science Foundation through award IIP-2016516. Partial support for the manufacturing prototyping run was provided by the Berthiaume Institute for Precision Health. Thanks to Alyssa Wicks, Kathleen Hayes, Awosiji Olatunde Awotunde, and Ornella Joseph for reading PADs in the blinded study. Special thanks to the Sakaue lab at Notre Dame for the use of their contact angle goniometer, to Adam Heet at the Navari Center for Digital Scholarship for laser cutting, and to Serim Research Corp. for prototyping materials, helpful discussions, and the use of their equipment.

Notes and references

- 1 A. W. Martinez, S. T. Phillips, M. J. Butte and G. M. Whitesides, *Angewandte Chemie - International Edition*, 2007, **46**, 1318–1320.
- 2 A. Apilux, W. Dungchai, W. Siangproh, N. Praphairaksit, C. S. Henry and O. Chailapakul, *Anal Chem*, 2010, **82**, 1727–1732.
- 3 B. M. Jayawardane, I. D. McKelvie and S. D. Kolev, *Talanta*, 2012, **100**, 454–460.
- 4 L. J. Loh, G. C. Bandara, G. L. Weber and V. T. Remcho, *Analyst*, 2015, **140**, 5501–5507.
- 5 T. Satarpai, J. Shiowatana and A. Siripinyanond, *Talanta*, 2016, **154**, 504–510.
- 6 B. Wang, Z. Lin and M. Wang, *J Chem Educ*, 2015, **92**, 733–736.
- 7 A. Chatmontree, S. Chairam, S. Supasorn, M. Amatongchai, P. Jarujamrus, S. Tamuang and E. Somsook, *J Chem Educ*, 2015, **92**, 1044–1048.
- 8 S. A. Nogueira, L. R. Sousa, N. K. L. Silva, P. H. F. Rodrigues and W. K. T. Coltro, *Micromachines (Basel)*, 2017, **8**, 1–10.
- 9 L. A. Barrera, A. C. Escobosa, L. S. Alsaihati and J. C. Noveron, *J Chem Educ*, 2019, **96**, 165–168.
- 10 S. Armenta, F. A. Esteve-Turrillas and J. M. Herrero-Martínez, *J Chem Educ*, 2020, **97**, 3852–3857.
- 11 S. L. Bliese, D. O'Donnell, A. A. Weaver and M. Lieberman, *J Chem Educ*, 2020, **97**, 786–792.
- 12 R. M. Roller, S. Sumantakul, M. Tran, A. van Wyk, J. Zinna, D. A. Donelson, S. G. Finnegan, G. Foley, O. R. Frechette, J. Gaetgens, J. Jiang, K. C. Rinaolo, R. S. Cole, M. Lieberman, V. T. Remcho and K. A. Frederick, *J Chem Educ*, 2021, **98**, 1946–1953.
- 13 V. D. E. Schmuck, I. C. Romine, T. A. Sisley, C. E. Immoos, G. E. Scott, D. F. Zigler and A. W. Martinez, *J Chem Educ*, 2022, **99**, 1081–1086.
- 14 J. Huang and L. Cai, *J Chem Educ*, 2022, **99**, 3607–3612.
- 15 A. A. Weaver, H. Reiser, T. Barstis, M. Benvenuti, D. Ghosh, M. Hunckler, B. Joy, L. Koenig, K. Raddell and M. Lieberman, *Anal Chem*, 2013, **85**, 6453–6460.
- 16 E. C. Tackman, M. J. Trujillo, T. L. E. Lockwood, G. Merga, M. Lieberman and J. P. Camden, *Analytical Methods*, 2018, **10**, 4718–4722.
- 17 S. L. Bliese, M. Maina, P. Were and M. Lieberman, *Analytical Methods*, 2019, **11**, 4727–4732.
- 18 I. Chikowe, S. L. Bliese, S. Lucas and M. Lieberman, *Am J Trop Med Hyg*, 2018, **99**, 233–238.
- 19 H.-H. Chen, C. Higgins, S. K. Laing, S. L. Bliese, M. Lieberman and S. Ozawa, *Medicine Access @ Point of Care*, 2021, **5**, 1–11.
- 20 N. M. Myers, M. W. Maina, M. Were, R. Karwa, S. D. Pastakia, J. C. Sharp, J. L. Luther, A. Cooper, S. L. Bliese, N. Oberhof and M. Lieberman, *Analytical Methods*, 2019, **11**, 4741–4750.
- 21 M. Smith, A. Ashenef and M. Lieberman, *J Glob Oncol*, 2018, 1–10.
- 22 M. S. Eberle, A. Ashenef, H. Gerba, P. J. Loehrer and M. Lieberman, *J Glob Oncol*, 2020, **6**, 407–413.
- 23 A. W. Martinez, S. T. Phillips, G. M. Whitesides and E. Carrilho, *Anal Chem*, 2010, **82**, 3–10.
- 24 A. W. Martinez, S. T. Phillips, Z. Nie, C. M. Cheng, E. Carrilho, B. J. Wiley and G. M. Whitesides, *Lab Chip*, 2010, **10**, 2499–2504.
- 25 A. K. Yetisen, M. S. Akram and C. R. Lowe, *Lab Chip*, 2013, **13**, 2210–2251.
- 26 C. R. Mace and R. N. Deraney, *Microfluid Nanofluidics*, 2014, **16**, 801–809.
- 27 J. C. Brooks and C. R. Mace, *J Anal Test*, 2019, **3**, 50–60.
- 28 Q. He, C. Ma, X. Hu and H. Chen, *Anal Chem*, 2013, **85**, 1327–1331.
- 29 B. Chen, P. Kwong and M. Gupta, *ACS Appl Mater Interfaces*, 2013, **5**, 12701–12707.
- 30 X. Li, J. Tian, T. Nguyen and W. Shen, *Anal Chem*, 2008, **80**, 9131–9134.
- 31 P. K. Kao and C. C. Hsu, *Microfluid Nanofluidics*, 2014, **16**, 811–818.
- 32 W. Wang, W. Y. Wu, W. Wang and J. J. Zhu, *J Chromatogr A*, 2010, **1217**, 3896–3899.
- 33 D. Zhang, L. Yan, Y. Zhang, T. Li and J. Wang, *Food Front*, 2020, **1**, 192–199.
- 34 R. Lu, W. Shi, L. Jiang, J. Qin and B. Lin, *Electrophoresis*, 2009, **30**, 1497–1500.
- 35 J. Nie, Y. Zhang, L. Lin, C. Zhou, S. Li, L. Zhang and J. Li, *Anal Chem*, 2012, **84**, 6331–6335.

- 36 N. K. Mani, A. Prabhu, S. K. Biswas and S. Chakraborty, *Sci Rep*, 2019, **9**, 1–8.
- 37 B. Gao, J. Chi, H. Liu and Z. Gu, *Sci Rep*, 2017, **7**, 1–8.
- 38 D. A. Bruzewicz, M. Reches and G. M. Whitesides, *Anal Chem*, 2008, **80**, 3387–3392.
- 39 C. Gallibu, C. Gallibu, A. Avoundjian and F. Gomez, *Micromachines (Basel)*, 2016, **7**, 6.
- 40 N. Nuchtavorn and M. Macka, *Anal Chim Acta*, 2016, **919**, 70–77.
- 41 E. M. Fenton, M. R. Mascarenas, G. P. López and S. S. Sibbett, *ACS Appl Mater Interfaces*, 2009, **1**, 124–129.
- 42 J. M. Pearce, N. C. Anzalone and C. L. Heldt, *J Lab Autom*, 2016, **21**, 510–516.
- 43 C. K. Chiang, A. Kurniawan, C. Y. Kao and M. J. Wang, *Talanta*, 2019, **194**, 837–845.
- 44 H. Yagoda, *Industrial and Engineering Chemistry - Analytical Edition*, 1937, **9**, 79–82.
- 45 R. H. Müller and D. L. Clegg, *Anal Chem*, 1949, **21**, 1123–1125.
- 46 Y. Zhang, C. Zhou, J. Nie, S. Le, Q. Qin, F. Liu, Y. Li and J. Li, *Anal Chem*, 2014, **86**, 2005–2012.
- 47 V. F. Curto, N. Lopez-Ruiz, L. F. Capitan-Vallvey, A. J. Palma, F. Benito-lopez and D. Diamond, *RSC Adv*, 2013, **3**, 18811–18816.
- 48 K. L. Dornelas, N. Dossi and E. Piccin, *Anal Chim Acta*, 2015, **858**, 82–90.
- 49 Y. He, Y. Wu, X. Xiao, J. Fu and G. Xue, *RSC Adv*, 2014, **4**, 63860–63865.
- 50 T. Songjaroen, W. Dungchai, O. Chailapakul and W. Laiwattanapaisal, *Talanta*, 2011, **85**, 2587–2593.
- 51 T. Nurak, N. Praphairaksit and O. Chailapakul, *Talanta*, 2013, **114**, 291–296.
- 52 M. Deng, C. Liao, X. Wang, S. Chen, F. Qi, X. Zhao and P. Yu, *Can J Chem*, 2019, **97**, 373–377.
- 53 W. Dungchai, O. Chailapakul and C. S. Henry, *Analyst*, 2011, **136**, 77–82.
- 54 S. Mohammadi, M. Maeki, R. M. Mohamadi, A. Ishida, H. Tani and M. Tokeshi, *Analyst*, 2015, **140**, 6493–6499.
- 55 P. Kajornklin, P. Jarujamrus, P. Phanphon, P. Ngerpradab, S. Supasorn, S. Chairam and M. Amatatongchai, *J Chem Educ*, 2020, **97**, 1984–1991.
- 56 Y. Sameenoi, P. Na Nongkai, S. Nouanthavong, C. S. Henry and D. Nacaprich, *Analyst*, 2014, **139**, 6580–6588.
- 57 E. Carrilho, A. W. Martinez and G. M. Whitesides, *Anal Chem*, 2009, **81**, 7091–7095.
- 58 J. S. Ng and M. Hashimoto, *RSC Adv*, 2020, **10**, 29797–29807.
- 59 R. Dey, S. Kar and S. Joshi, *Microfluid Nanofluidics*, 2015, **19**, 375–383.
- 60 R. Ghosh, S. Gopalakrishnan, R. Savitha and T. Renganathan, *Sci Rep*, 2019, **9**, 1–11.
- 61 C. G. Shi, X. Shan, Z. Q. Pan, J. J. Xu, C. Lu, N. Bao and H. Y. Gu, *Anal Chem*, 2012, **84**, 3033–3038.
- 62 K. Abe, K. Suzuki and D. Citterio, *Anal Chem*, 2008, **80**, 6928–6934.
- 63 X. Li, J. Tian, G. Garnier and W. Shen, *Colloids Surf B Biointerfaces*, 2010, **76**, 564–570.
- 64 A. Määttänen, D. Fors, S. Wang, D. Valtakari, P. Ihalainen and J. Peltonen, *Sens Actuators B Chem*, 2011, **160**, 1404–1412.
- 65 J. Wang, M. R. N. Monton, X. Zhang, C. D. M. Filipe, R. Pelton and J. D. Brennan, *Lab Chip*, 2014, **14**, 691–695.
- 66 V. Rajendra, C. Sicard, J. D. Brennan and M. A. Brook, *Analyst*, 2014, **139**, 6361–6365.
- 67 C. Xu, L. Cai, M. Zhong and S. Zheng, *RSC Adv*, 2015, **5**, 4770–4773.
- 68 K. Maejima, S. Tomikawa, K. Suzuki and D. Citterio, *RSC Adv*, 2013, **3**, 9258–9263.
- 69 R. A. Ruiz, J. L. Gonzalez, M. Vazquez-Alvarado, N. W. Martinez and A. W. Martinez, *Anal Chem*, 2022, **94**, 8833–8837.
- 70 J. Greener, in *Roll-to-Roll Manufacturing: Process Elements and Recent Advances*, eds. J. Greener, M. Cakmak and G. Pearson, John Wiley & Sons, 2018, pp. 1–17.
- 71 G. Jenkins, Y. Wang, Y. L. Xie, Q. Wu, W. Huang, L. Wang and X. Yang, *Microfluid Nanofluidics*, 2015, **19**, 251–261.
- 72 S. Lutz, P. Weber, M. Focke, B. Faltin, J. Hoffmann, C. Müller, D. Mark, G. Roth, P. Munday, N. Armes, O. Piepenburg, R. Zengerle and F. von Stetten, *Lab Chip*, 2010, **10**, 887–893.
- 73 J. Olkkonen, K. Lehtinen and T. Erho, *Anal Chem*, 2010, **82**, 10246–10250.
- 74 J. Songok, M. Tuominen, H. Teisala, J. Haapanen, J. Mäkelä, J. Kuusipalo and M. Toivakka, *ACS Appl Mater Interfaces*, 2014, **6**, 20060–20066.
- 75 J. Liu, X. Kong, H. Wang, Y. Zhang and Y. Fan, *Microfluid Nanofluidics*, 2020, **24**, 1–7.
- 76 E. Fu, B. Lutz, P. Kauffman and P. Yager, *Lab Chip*, 2010, **10**, 918–920.
- 77 P. Kauffman, E. Fu, B. Lutz and P. Yager, *Lab Chip*, 2010, **10**, 2614–2617.
- 78 I. Jang, K. E. Berg and C. S. Henry, *Sens Actuators B Chem*, 2020, **319**, 1–8.
- 79 A. Demesie, MSc Thesis, Addis Ababa University, 2022.
- 80 M. Chanie, MSc Thesis, Addis Ababa University, 2022.
- 81 T. L. E. Lockwood, T. X. Leong, S. L. Bliese, A. Helmke, A. Richard, G. Merga, J. Rorabeck and M. Lieberman, *J Forensic Sci*, 2020, **65**, 1289–1297.
- 82 E. W. Washburn, *Physical Review*, 1921, **18**, 273–283.
- 83 Z. W. Zhong, Z. P. Wang and G. X. D. Huang, *Microsyst Technol*, 2012, **18**, 649–659.
- 84 C. A. Schneider, W. S. Rasband and K. W. Eliceiri, *Nat Methods*, 2012, **9**, 671–675.
- 85 S. Banerjee, J. Sweet, C. Sweet and M. Lieberman, in *2016 IEEE Winter Conference on Applications of*

- Computer Vision, WACV 2016*, Institute of Electrical and Electronics Engineers Inc., 2016.
- 86 Paper Analytics LLC, 2022.
- 87 H. Liu, Y. Xiang, Y. Lu and R. M. Crooks, *Angewandte Chemie - International Edition*, 2012, **51**, 6925–6928.
- 88 J. Zinna, T. L. E. Lockwood and M. Lieberman, *Analytical Methods*, 2020, **12**, 1077–1084.
- 89 S. K. Biswas, S. Chatterjee, S. Bandyopadhyay, S. Kar, N. K. Som, S. Saha and S. Chakraborty, *ACS Sens*, 2021, **6**, 1077–1085.
- 90 J. Prabpal, T. Vilaivan and T. Praneenararat, *J Chem Educ*, 2017, **94**, 1137–1142.
- 91 M. Srisa-Art, K. E. Boehle, B. J. Geiss and C. S. Henry, *Anal Chem*, 2018, **90**, 1035–1043.
- 92 P. Namwong, P. Jarujamrus, M. Amatatongchai and S. Chairam, *J Chem Educ*, 2018, **95**, 305–309.
- 93 S. H. Yeh, K. H. Chou and R. J. Yang, *Lab Chip*, 2016, **16**, 925–931.
- 94 K. Tenda, R. Ota, K. Yamada, T. G. Henares, K. Suzuki and D. Citterio, *Micromachines (Basel)*, , DOI:10.3390/mi7050080.
- 95 C. L. Sones, I. N. Katis, P. J. W. He, B. Mills, M. F. Namiq, P. Shardlow, M. Ibsen and R. W. Eason, *Lab Chip*, 2014, **14**, 4567–4574.